

Heterogeneous Interactions of ClONO₂ and HCl with Sulfuric Acid Tetrahydrate: Implications for the Stratosphere

Renyi Zhang, John T. Jayne, and Mario J. Molina*

Department of Earth, Atmospheric and Planetary Sciences and Department of Chemistry,
Massachusetts Institute of Technology, Cambridge, Massachusetts 02139

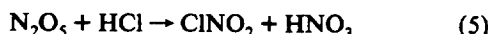
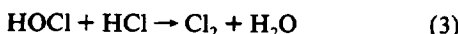
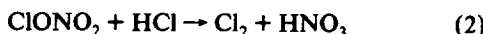
Received: August 13, 1993; In Final Form: October 20, 1993*

110-46-12
7N-46-12
Cited
043 451

The reaction probabilities for ClONO₂ + H₂O → HOCl + HNO₃ (1) and ClONO₂ + HCl → Cl₂ + HNO₃ (2) have been investigated on sulfuric acid tetrahydrate (SAT, H₂SO₄·4H₂O) surfaces at temperatures between 190 and 230 K and at reactant concentrations that are typical in the lower stratosphere, using a fast-flow reactor coupled to a quadrupole mass spectrometer. The results indicate that the reaction probabilities as well as HCl uptake depend strongly on the thermodynamic state of SAT surface: they decrease significantly with decreasing H₂O partial pressure at a given temperature, and decrease with increasing temperature at a given H₂O partial pressure, as the SAT changes from the H₂O-rich form to the H₂SO₄-rich form. For H₂O-rich SAT at 195 K $\gamma_1 \approx 0.01$ and $\gamma_2 \geq 0.1$, whereas the values for H₂SO₄-rich SAT decrease by more than 2 orders of magnitude. At low concentrations of HCl, close to those found in the stratosphere, the amount of HCl taken up by H₂O-rich SAT films corresponds to a coverage of the order of a tenth of a monolayer ($\approx 10^{14}$ molecules cm⁻²); H₂SO₄-rich SAT films take up 2 orders of magnitude less HCl ($< 10^{12}$ molecules cm⁻²). Substantial HCl uptake at high HCl concentrations is also observed, as a result of surface melting. The data reveal that frozen stratospheric sulfate aerosols may play an important role in chlorine activation in the winter polar stratosphere via processes similar to those occurring on the surfaces of polar stratospheric cloud particles.

Introduction

It is now well established that stratospheric ozone depletion in the polar regions as well as on a global scale is largely the result of heterogeneous processes occurring on the surfaces of stratospheric particles.^{1–4} The heterogeneous reactions of primary interest in the stratosphere are as follows:



The important consequence of these reactions is that the relatively inert chlorine reservoir molecules (ClONO₂, HCl) are converted into forms (Cl₂, ClONO₂) that release chlorine radicals readily upon photolysis. The concomitant suppression of gas-phase reactive nitrogen radicals (NO_x) is also crucial to the efficiency of ozone destruction since they react with halogen radicals to form relatively stable reservoir species, halting ozone depletion.

The stratospheric particles which act as catalysts for these reactions are either background sulfate aerosols or polar stratospheric cloud particles. Two distinct types of polar stratospheric clouds (PSCs) have been proposed: type I is usually assumed to consist of nitric acid trihydrate and type II to consist of water ice;^{5–8} background stratospheric aerosols at mid-latitudes are liquid and are composed mainly of 60–80 wt % aqueous H₂SO₄.⁹ Recent laboratory¹⁰ and field¹¹ studies suggest that at low temperatures ($T < 200$ K) such as those prevailing in the early polar winter stratospheric aerosols are composed of supercooled HNO₃/H₂SO₄/H₂O ternary solutions. Also, laboratory work^{12–14} reveals that crystalline sulfuric acid hydrates may form and persist under

temperature and water partial pressure conditions typical of the high-latitude stratosphere.

There have been several laboratory kinetic studies of reactions 1–4 on various proposed stratospheric materials; the reaction probabilities (γ 's) have been measured on water ice,^{15–19} on NAT,^{20–25} and on liquid sulfuric acid solutions.^{13,26,27} In particular, reactions 1 and 2 have been shown to occur readily at stratospheric concentrations of ClONO₂ and HCl on surfaces of water ice and NAT in coexistence with ice^{22,24} and to vary strongly as a function of the thermodynamic state of the NAT surfaces.²⁵ Heterogeneous reactions occurring on frozen sulfuric acid surfaces were, however, previously thought to be of relatively little importance in the stratosphere; in particular, reaction 4 occurs readily on liquid sulfate aerosols, but it is very inefficient on the frozen particles.²⁶

In this paper we report measurements of the reaction probabilities of (1) and (2) on sulfuric acid tetrahydrate (SAT) surfaces, conducted at reactant partial pressures characteristic of the stratosphere, that is, on the order of 10⁻⁸–10⁻⁷ Torr for ClONO₂ and HCl. Our results indicate that the reaction probabilities as well as HCl uptake depend strongly on the thermodynamic state of the SAT surface, which is determined by the temperature and H₂O partial pressure in equilibrium with the solid.¹² The H₂O-rich forms are shown to be more reactive than the H₂SO₄-rich forms. At high HCl partial pressures substantial HCl uptake is observed, most likely as a result of substrate melting. The data reveal that frozen stratospheric sulfate aerosols play an important role in chlorine activation in the winter polar stratosphere via processes similar to those occurring on PSC surfaces.

Experimental Section

The experiments were performed in a newly constructed apparatus shown schematically in Figure 1, which consists of a tubular fast-flow reactor coupled to a differentially pumped, molecular beam sampling quadrupole mass spectrometer (Exrel EXM-200) for species detection. In this configuration the main gas flow was pumped by a roughing pump (Edwards Model E2M80, 27 L s⁻¹ pumping speed). A small fraction of the main

* Abstract published in Advance ACS Abstracts, December 15, 1993.

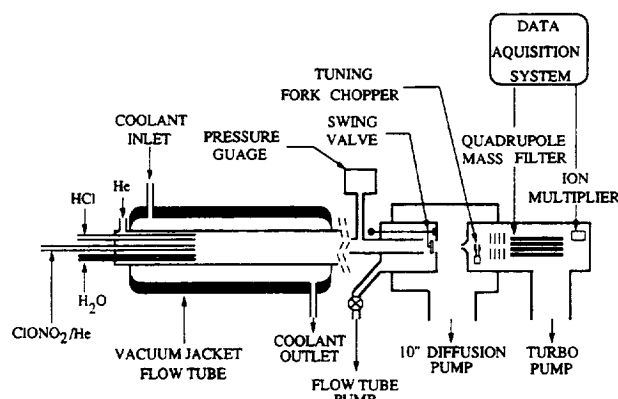


Figure 1. Schematic diagram of the experimental apparatus.

gas flow passed through a 0.1-cm-diameter pinhole into a chamber evacuated by a 10-in. diffusion pump (Edwards Model CR 250). The gas diffusing through this pinhole was collimated by a 0.1-cm-diameter skimmer cone (Beam Dynamics) mounted on the front of the vacuum chamber which housed the mass spectrometer. The two pinholes were separated by a distance of about 0.7 cm. The resulting molecular beam was modulated at 200 Hz by a tuning fork chopper before entering an electron impact ionization region to produce positive ions. The mass-filtered ions were collected at a conversion dynode and further amplified by the Channeltron electron multiplier, an Extrel electrometer, and, when phase-sensitive detection is employed, a lock-in amplifier (EG&G PAR Model 5209). The mass spectrometer chamber was evacuated by a turbomolecular pump (Seiko-Seiki Model STP-400, 400 L s⁻¹). With 1 Torr total pressure in the flow reactor the pressures in the diffusion pumped chamber and the mass spectrometer chamber were 5×10^{-5} and 3×10^{-6} Torr, respectively. Under these operating conditions the pressure in the ionizer (the molecular beam pressure) was about 4 times greater than the chamber pressure, as determined by a separate set of experiments. The sensitivity of this system was tested using SF₆ as an inert tracer species: with 1 Torr total pressure of helium in the flow tube the partial pressure of SF₆ detected with a S/N ratio of 2 was about 1×10^{-8} Torr.

The flow tube can be isolated from the mass spectrometer system by rotating a small O-ring seal valve with a spring-loaded closure mechanism to cover the pinhole. This design facilitated the coupling of the flow tube to the mass spectrometer with minimal spacing and provided a convenient way for removing the flow tube for treatments, such as coating its inside wall with liquid H₂SO₄ solutions.

Two different 50-cm-length flow tubes were employed in the experiments: the inner diameters are 2.2 and 2.8 cm, respectively. Both flow tubes are surrounded by inner jackets in which refrigerated ethanol is circulated. The outer jackets of the flow tubes are evacuated to provide thermal insulation. Three movable injectors are located at the upstream end of the flow tube: a jacketed injector (1.0-cm o.d.) kept warm by flowing a room temperature solution of ethylene glycol in water to add water vapor to the system, a center-located injector (0.3-cm o.d.) to introduce the reactant, and an injector (0.3-cm o.d.) to introduce other trace gas species such as HCl. To prevent possible warming of the substrate by the jacketed injector, water was added to the system near the upstream end of the flow tube. The ethanol reservoir used to cool the flow tube was temperature-regulated by a combination of resistance heating and liquid nitrogen cooling. The coolant temperature was monitored with thermocouples located at the entrance and exit of the cooling jacket. The temperature of the refrigeration system could be maintained or regulated between 190 and 230 K: the stability of the system was about ± 0.5 °C. Typically, the temperature variation over the length of the flow tube was less than 1 K.

For all experiments reported here the flow tube was operated at pressures between 0.5 and 2.0 Torr, and the average buffer gas (helium) velocities ranged from 1100 to 2000 cm s⁻¹. Gas flows were monitored by electronic mass flow meters (Tylan Model FM-360), and the total flow tube pressure was monitored by a 10-Torr full scale pressure transducer (MKS Model 220CA) with an accuracy of ± 0.5 mTorr.

SAT surfaces were prepared by completely covering the inside wall of the flow tube with a liquid film of ~ 57.7 wt % H₂SO₄ solution and by quickly cooling the film to low temperatures. To ensure uniform wetting, the flow tube was first cleaned with a dilute HF solution or with a chromic-sulfuric acid solution and then rinsed with distilled water; the thickness of the films was typically greater than 0.1 mm. Crystallization of the liquid coating normally occurred at about 200 K upon cooling, and the SAT surfaces were verified to melt within a degree of the pure SAT melting point.²⁸ Generally, upon freezing, the solid exhibited H₂O vapor pressures very close to those of pure ice, characteristic of the coexistence mixture of ice/tetrahydrate. By slowly raising the temperature and by flowing dry helium over the samples, a sudden drop in the water vapor pressure was observed after some time, suggesting that the ice phase had evaporated, leaving only SAT behind. The H₂SO₄-rich and H₂O-rich forms of the tetrahydrate could then be generated by controlling the equilibrium H₂O vapor pressure through addition or evaporation of small amounts of water at a constant temperature or by controlling the temperature at a constant H₂O partial pressure.¹² Ice films were prepared by depositing a known amount of H₂O vapor at 195 K and were calculated to be approximately 15–25 μ m thick.

Reaction probabilities (γ) were calculated from first-order rate constants (k) corresponding to the reactant loss or product growth:

$$\gamma = 2rk/(\omega + rk) \quad (6)$$

where r is the radius of the flow tube and ω is the mean thermal speed of the reactant. To account for the ClONO₂ radial gradients in the flow tube which arise when there is a large reactant wall loss, the observed first-order rate constants (k_{obs}) were corrected for gas diffusion by the method suggested by Brown to obtain k .²⁹ The ClONO₂ diffusion coefficient in helium used in the Brown calculations was 176 cm²/s at 200 K and 1 Torr, with a temperature dependency of $T^{1.76}$ and a pressure dependency of P^{-1} , respectively.³⁰ These corrections were approximately 10% for small γ values ($\gamma < 0.01$) and as large as a factor of 4 for large γ 's ($\gamma > 0.2$).

ClONO₂ was synthesized by the reaction between ClF and HNO₃, according to the procedure described by Schack.³¹ The purity of ClONO₂ samples was checked both by ultraviolet spectrophotometry at several wavelengths and by mass spectrometry and was found to be greater than 90% in the gas phase, with Cl₂ being the major impurity. To deliver ClONO₂ to the flow tube, 0.5–10 cm³ min⁻¹ of helium passed through a ClONO₂ bubbler maintained at 195 K in a dry ice-acetone bath. The concentration of ClONO₂, prior to passing through a needle valve and entering the flow tube, was determined by UV absorption at 220 nm (cross section = 3.44×10^{-18} cm²).³² Water signals were calibrated over the temperature range of 190–230 K by depositing an ice film from H₂O vapor and calculating its vapor pressure from the relationship given by Jansco et al.³³ HCl was introduced to the flow tube from a dilute mixture in helium (0.5%), and its concentration was determined either by observing the pressure rise in the flow system upon its addition or by using a 10 cm³ min⁻¹ mass flow meter. HCl, ClONO₂, HOCl, and Cl₂ were monitored at mass peaks of 36, 46 (by detection of the NO₂⁺ ion fragment at $m/e = 46$), 52, and 70, respectively. Detection limits were 10^{-8} Torr for ClONO₂, HOCl, and Cl₂ and 10^{-5} Torr for H₂O. The detection sensitivity was limited mainly by the background partial pressure. The mass spectrometer signals,

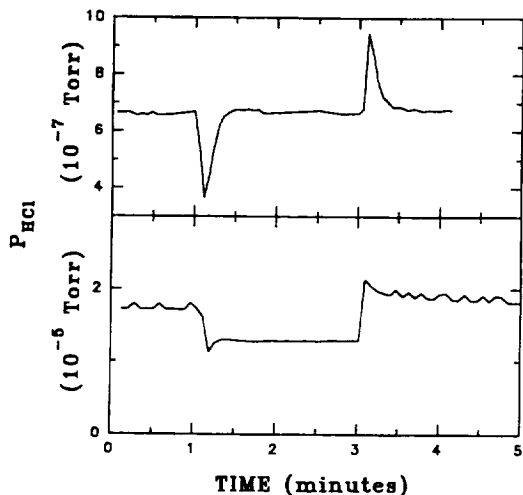


Figure 2. Time evolution of the HCl signal for two typical HCl uptake experiments on SAT at 195 K and $P_{\text{H}_2\text{O}} = 4 \times 10^{-4}$ Torr: (top trace) $P_{\text{HCl}} = 6.7 \times 10^{-7}$ Torr and (bottom trace) $P_{\text{HCl}} = 2 \times 10^{-5}$ Torr. The injector is pulled upstream by 5 cm at 1 min and returned to its original position at 3 min.

the flows, the total pressure, and the temperature were recorded by a computer data acquisition system.

Results

HCl Uptake Experiments. The uptake of HCl by SAT films was studied using the method previously described.^{24,25,34} Briefly, a steady-state flow of HCl in helium was first established through one of the unjacketed injectors pushed in just pass the solid sulfuric acid film. The injector was then quickly pulled upstream exposing 3–10-cm length of the film to HCl while monitoring the HCl signal in the mass spectrometer. Uptake from the gas phase was determined from the decline and recovery in the HCl signal and the flow rates.

Figure 2 shows time evolution of the HCl signal for two typical uptake experiments performed at 195 K and $P_{\text{H}_2\text{O}} = 4 \times 10^{-4}$ Torr: the injector is pulled 5 cm upstream at 1.0 min and returned to its original position at 3.0 min. For the case of the small HCl partial pressure ($\sim 6.7 \times 10^{-7}$ Torr), the HCl signal falls from its initial steady-state value as HCl is taken up by the SAT film and later returns as the surface layer becomes saturated with HCl; pushing back the injector results in HCl desorption, with a peak similar to the uptake peak (top trace). The total number of HCl molecules taken up is calculated to be $\sim 1.5 \times 10^{14}$ molecules cm^{-2} , assuming a SAT surface area equal to the geometrical area of the flow tube. Clearly, the actual coverage is smaller because of surface roughness and porosity; surface morphology studies will be needed to accurately determine the surface area. For the high initial HCl partial pressure (2×10^{-5} Torr) the HCl signal drops substantially on pulling the injector upstream and does not recover to its starting level on the time scale of minutes, probably indicating that surface melting occurs (bottom trace).

The dependence of the HCl uptake on its partial pressure is illustrated in Figure 3 over the range of HCl partial pressures from 3×10^{-7} to 2×10^{-5} Torr. The temperature and H₂O partial pressure are kept constant at 195 K, and $P_{\text{H}_2\text{O}} = 4.5 \times 10^{-4}$ Torr during these experiments. A threshold HCl partial pressure, above which melting occurs, is identified at $\sim 1.5 \times 10^{-5}$ Torr under those conditions.

Figure 4 shows results of the HCl uptake as a function of the H₂O partial pressure at 195 K and at a fixed HCl partial pressure of $\sim 5 \times 10^{-7}$ Torr. We have previously suggested that in an isothermal experiment a readjustment of the H₂O partial pressure in the flow tube is followed by a corresponding change in the

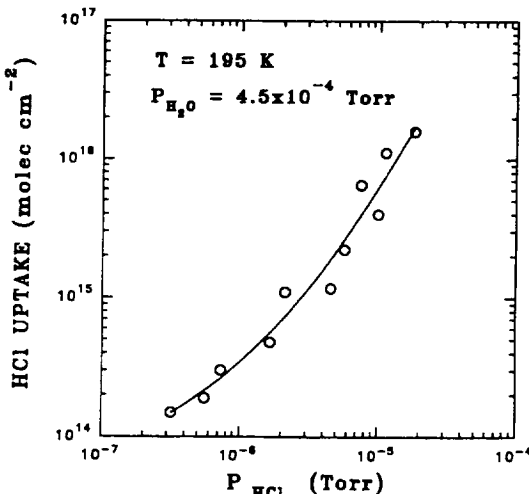


Figure 3. HCl surface coverages on SAT films as a function of P_{HCl} at 195 K and $P_{\text{H}_2\text{O}} = 4.5 \times 10^{-4}$ Torr. The solid curve is a fit of the experimental data in the form of eq 7 and is also summarized in Table 1.

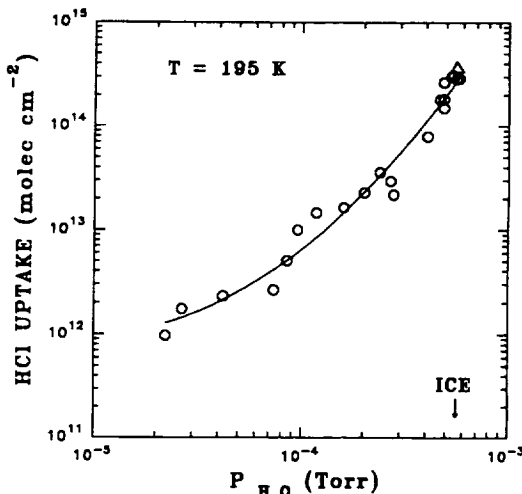


Figure 4. HCl surface coverages on SAT films as a function of $P_{\text{H}_2\text{O}}$ at 195 K and $P_{\text{HCl}} \approx 5 \times 10^{-7}$ Torr. Also shown in this figure is the result of HCl uptakes measured on fresh ice films (open triangle, average of nine experiments). The ice vapor pressure at this temperature is labeled. The solid curve is a fit of the experimental data in the form of eq 7 and is also summarized in Table 1.

thermodynamic state—and hence the composition—of the SAT film, occurring mostly in its surface layers.¹² As shown in this figure, the HCl uptake exhibits a strong dependence on the thermodynamic state of SAT: the H₂O-rich forms take up more than 2 orders of magnitude as much HCl than the H₂SO₄-rich forms. When the H₂O partial pressure over the SAT film approaches that of pure ice, characteristic of the coexistence mixture of ice/tetrahydrate, the uptake resembles that observed on fresh ice films for the same temperature and HCl partial pressure conditions (open triangle, average of nine experiments).

To simulate the temperature dependence of the HCl uptake under stratospheric conditions, we investigated the uptake by keeping the H₂O partial pressure constant and by varying the temperature in the flow tube, a process which also involves the transformation of H₂O-rich to H₂SO₄-rich hydrate as the substrate is warmed from 192 to 218 K at the particular H₂O partial pressure of the experiment (3.4×10^{-4} Torr).¹² Figure 5 gives the results of these experiments at a fixed P_{HCl} ($\sim 6 \times 10^{-7}$ Torr) as a function of temperature. As shown in this figure, at high temperatures ($T > 200$ K) the SAT film takes up only very small amount of

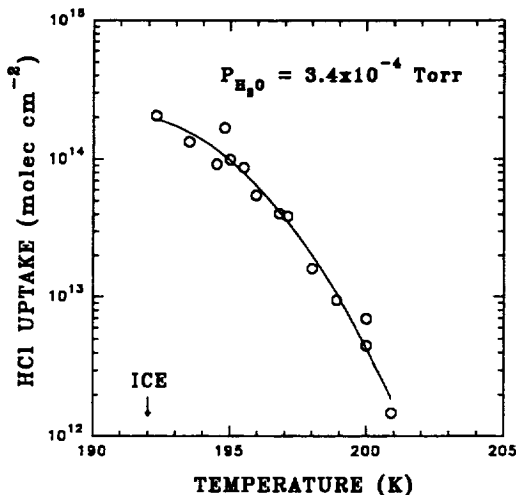


Figure 5. HCl surface coverages on SAT films as a function of temperature at $P_{\text{H}_2\text{O}} = 3.4 \times 10^{-4}$ Torr and $P_{\text{HCl}} \approx 6 \times 10^{-7}$ Torr. The ice frost point is labeled. The solid curve is a fit of the experimental data in the form of eq 7 and is also summarized in Table 1.

TABLE 1: Summary and Parametrization^a of the HCl Uptake Experiments

variable x	coefficient			experimental conditions
	a_1	a_2	a_3	
P_{HCl} (Torr)	32.58	5.11	0.35	$T = 195$ K $P_{\text{HCl}} = 3 \times 10^{-7} - 2 \times 10^{-5}$ Torr $P_{\text{H}_2\text{O}} = 4.5 \times 10^{-4}$ Torr
$P_{\text{H}_2\text{O}}$ (Torr)	31.56	7.79	0.78	$T = 195$ K $P_{\text{HCl}} \approx 5 \times 10^{-7}$ Torr $P_{\text{H}_2\text{O}} = 2 \times 10^{-5} - 5.6 \times 10^{-4}$ Torr
T (K)	-788.50	7.99	-0.02	$T = 192 - 201$ K $P_{\text{HCl}} \approx 6 \times 10^{-7}$ Torr $P_{\text{H}_2\text{O}} = 3.4 \times 10^{-4}$ Torr

^a $\log S_{\text{HCl}} = a_1 + a_2 \log x + a_3 \log^2 x$. S_{HCl} in molecules cm^{-2} .

HCl ($< 10^{13}$ molecules cm^{-2}) whereas the uptake approaches $\sim 10^{14}$ molecules cm^{-2} at low temperatures ($T < 195$ K).

For convenience in presentation, the data shown in Figures 3–5 are also summarized in Table 1: the surface coverage of HCl (S_{HCl}) is fitted by the following functional form:

$$\log S_{\text{HCl}} = a_1 + a_2 \log x + a_3 \log^2 x \quad (7)$$

where x can be replaced by P_{HCl} (Torr), $P_{\text{H}_2\text{O}}$ (Torr), or T (K); the coefficients a_j ($j = 1, 3$) for each fit are tabulated along with the corresponding experimental conditions.

Reaction of ClONO₂ with H₂O. Reaction probability (γ_1) measurements for the reaction between ClONO₂ and H₂O on SAT were conducted by observing the decay of ClONO₂ or the growth of HOCl as a function of the ClONO₂ injector position as it was pulled upstream over the SAT film.

A typical result of reactive uptake of ClONO₂ by a SAT film is shown in Figure 6 as the time evolution of ClONO₂ and HOCl signals: at ~ 0.8 min, a 20-cm length of SAT film is exposed to ClONO₂ by pulling the injector upstream, and the signal of ClONO₂ drops sharply to a very small value while the HOCl signal rises; at ~ 2 min, the injector is moved back downstream to stop the exposure, and both the ClONO₂ and HOCl signals return within a fraction of a second to their initial levels. As displayed in the figure, the product that leaves the surface is identified as HOCl; the other product, HNO₃, is left behind on the surface. (HNO₃ is also detected by the NO₂⁺ ion fragment

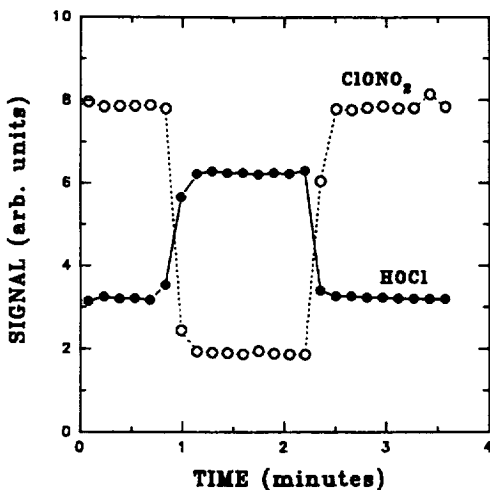


Figure 6. Time evolution of ClONO₂ ($m/e = 46$) and HOCl ($m/e = 52$) signals for a typical ClONO₂ reactive uptake experiment on SAT. Experimental conditions: $P_{\text{ClONO}_2} = 7 \times 10^{-8}$ Torr, $P_{\text{H}_2\text{O}} = 4 \times 10^{-4}$ Torr, $P_{\text{He}} = 0.8$ Torr, velocity = 1371 cm s^{-1} , $T = 195$ K.

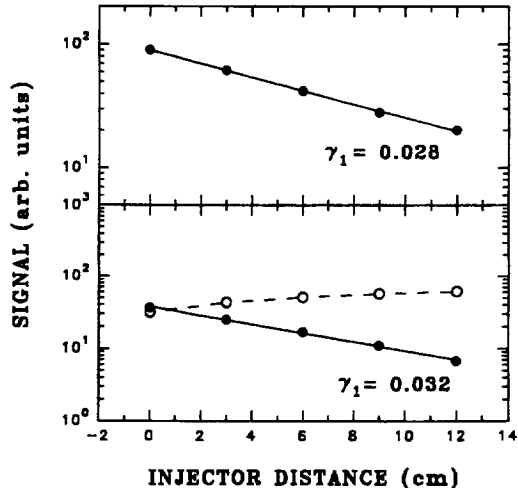


Figure 7. ClONO₂ (top) and HOCl (bottom, open circle) signals as a function of injector position. For the HOCl growth curve the first-order rate constant is calculated from the slope of a plot of $(S_{\text{HOCl}}(\infty) - S_{\text{HOCl}}(z))$ (solid curve), where $S_{\text{HOCl}}(\infty)$ is the HOCl signal at large injector distance (see text for details). Experimental conditions: $P_{\text{ClONO}_2} = 7 \times 10^{-8}$ Torr, $P_{\text{H}_2\text{O}} = 5.4 \times 10^{-4}$ Torr, $P_{\text{He}} = 1.0$ Torr, velocity = 1500 cm s^{-1} , and $T = 195$ K.

at $m/e = 46$.) In all of our experiments of this type, the maximum signal due to HOCl was always smaller than the initial ClONO₂ signal, suggesting some uptake of HOCl by the SAT surface. Since calibrations of the measured ClONO₂ and HOCl signals showed approximately the same relative sensitivities for detecting these two species in our mass spectrometer system, we estimate a lower limit of 50% for the yield of HOCl liberated into the gas phase.

Figure 7 shows a semilog plot of measured ClONO₂ and HOCl signals versus injector position for an experiment performed at 195 K and an initial ClONO₂ partial pressure of 7×10^{-8} Torr. For the ClONO₂ decay curve (top trace), the slope of the line yields the first-order rate constant; for the HOCl growth curve (bottom, solid line), the first-order rate constant is calculated from the slope of a plot of $(S_{\text{HOCl}}(\infty) - S_{\text{HOCl}}(z))$ versus injector distance, where z is the injector position and $S_{\text{HOCl}}(\infty)$ is the asymptotic HOCl signal at large injector distance, estimated visually from the figure. Both the ClONO₂ decay and HOCl growth follow first-order kinetics. The difference in the reaction probabilities obtained using both methods is negligible within experimental precision.

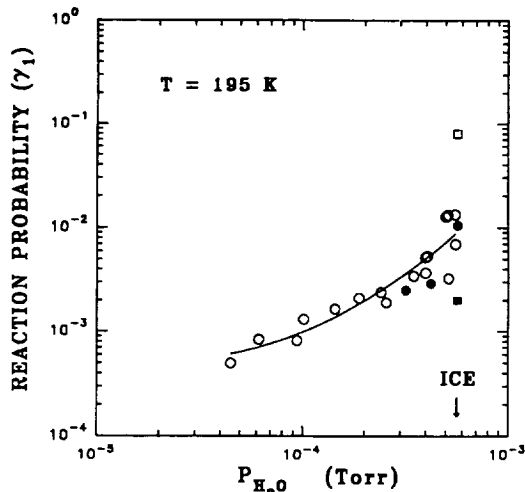


Figure 8. Reaction probability (γ_1) for reaction 1 (hydrolysis of ClONO₂) as a function of $P_{\text{H}_2\text{O}}$ on SAT surfaces at 195 K. Open circles are γ_1 's determined by the ClONO₂ decay, and solid circles are determined by the HOCl growth. The solid curve is a fit to the experimental data in a functional form similar to eq 7 and is also summarized in Table 2. Also shown in this figure are γ_1 's measured on fresh ice films (open square, average of 15 experiments) and on HNO₃-treated ice films (solid square, average of 11 experiments). The ice vapor pressure at this temperature is labeled. Experimental conditions: $P_{\text{ClONO}_2} = 3 \times 10^{-8}$ – 5×10^{-8} Torr, $P_{\text{He}} = 0.9$ – 1.0 Torr, velocity = 1300–1500 cm s⁻¹, and $T = 195$ K.

In Figure 8, values of γ_1 calculated from experiments such as those displayed in Figure 7 are presented as a function of $P_{\text{H}_2\text{O}}$ at 195 K ($P_{\text{ClONO}_2} = (3$ – $5) \times 10^{-8}$ Torr). It is seen that as the H₂O partial pressure approaches that of pure ice, i.e., for H₂O-rich SAT, γ_1 approaches 0.016; for low H₂O partial pressures (H₂SO₄-rich SAT) its value decreases by almost 2 orders of magnitude. Also shown in this figure are results of γ_1 measurements performed on freshly prepared ice surfaces (open square, average of 15 experiments) and on HNO₃-treated ice surfaces (solid square, average of 11 experiments) at the same temperature.

To demonstrate the effect of temperature on γ_1 under conditions pertinent to the stratosphere, a set of experiments was conducted on SAT films at a fixed H₂O pressure ($P_{\text{H}_2\text{O}} = 3.4 \times 10^{-4}$ Torr) and over a range of temperatures. These results are depicted in Figure 9 with the ClONO₂ partial pressures in the range (2–4) $\times 10^{-8}$ Torr. At high temperatures ($T > 205$ K), γ_1 is observed to be less than 10^{-3} , whereas it increases substantially at low temperatures ($\gamma_1 > 0.02$ at $T < 195$ K).

The data for γ_1 displayed in Figures 8 and 9 are also parametrized in the form of eq 7, and the coefficients are given in Table 2 along with the experimental conditions.

For all experiments described above, a freshly prepared SAT film was used for each measurement. Attempts were also made to examine the effect of flow tube radius on the γ_1 values: within experimental precision the results using the two flow tubes with different inner diameters were essentially the same. The estimated error limit of the γ_1 values is approximately $\pm 30\%$, which includes the uncertainties in measuring the first-order rate constant and in correcting the gas-phase diffusion. This error limit, however, does not include porosity and surface roughness effects, discussed below.

Reaction of ClONO₂ with HCl. We investigated the reactive uptake of ClONO₂ by SAT in the presence of HCl vapor: the measurements were performed by allowing the substrate to equilibrate with HCl vapor introduced into the flow tube with helium through one of the unjacketed injectors.

Figure 10 shows the ClONO₂ and Cl₂ signals as a function of time for a typical experiment conducted at 195 K and at a H₂O partial pressure of 4×10^{-4} Torr. The initial partial pressures of ClONO₂ and HCl for this experiment are 7×10^{-8} and $4 \times$

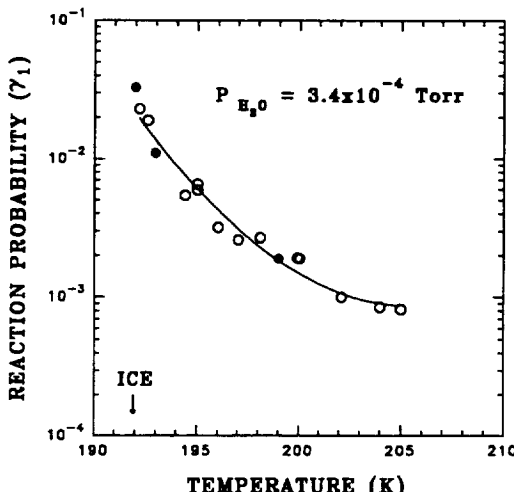


Figure 9. Reaction probability (γ_1) for reaction 1 (hydrolysis of ClONO₂) as a function of temperature on SAT surfaces. Open circles are γ_1 's determined by ClONO₂ decay, and solid circles are determined by HOCl growth. The solid curve is a fit to the experimental data in a functional form similar to eq 7 and is also summarized in Table 2. The ice frost point is labeled. Experimental conditions: $P_{\text{ClONO}_2} = 2 \times 10^{-8}$ – 4×10^{-8} Torr, $P_{\text{H}_2\text{O}} = 3.4 \times 10^{-4}$ Torr, $P_{\text{He}} = 0.9$ – 1.0 Torr, velocity = 1300–1600 cm s⁻¹, and $T = 195$ K.

TABLE 2: Summary and Parametrization^a of the γ_1 Measurements

variable x	coefficients			experimental conditions
	a_1	a_2	a_3	
$P_{\text{H}_2\text{O}}$ (Torr)	10.12	5.75	0.62	$T = 195$ K $P_{\text{ClONO}_2} = 3 \times 10^{-8}$ – 5×10^{-8} Torr $P_{\text{H}_2\text{O}} = 4 \times 10^{-5}$ – 5.6×10^{-4} Torr
T (K)	318.67	-3.13	0.0076	$T = 192$ – 206 K $P_{\text{ClONO}_2} = 2 \times 10^{-8}$ – 4×10^{-8} Torr $P_{\text{H}_2\text{O}} = 3.4 \times 10^{-4}$ Torr

$$^a \log \gamma_1 = a_1 + a_2 \log x + a_3 \log^2 x.$$

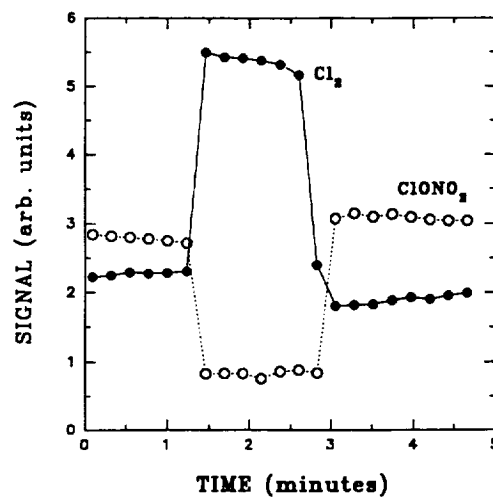


Figure 10. Time evolution of ClONO₂ ($m/e = 46$) and Cl₂ ($m/e = 70$) signals for a typical ClONO₂ reactive uptake experiment on SAT in the presence of HCl vapor. Experimental conditions: $P_{\text{ClONO}_2} = 7 \times 10^{-8}$ Torr, $P_{\text{H}_2\text{O}} = 4 \times 10^{-4}$ Torr, $P_{\text{HCl}} = 4 \times 10^{-7}$ Torr, $P_{\text{He}} = 1.3$ Torr, velocity = 1400 cm s⁻¹, and $T = 195$ K.

$\times 10^{-7}$ Torr, respectively. At 1.4 min the ClONO₂ injector is pulled upstream by 8 cm, and a pronounced time-independent decrease is observed in the ClONO₂ signal while the Cl₂ signal increases immediately. When the injector is pushed back to its starting

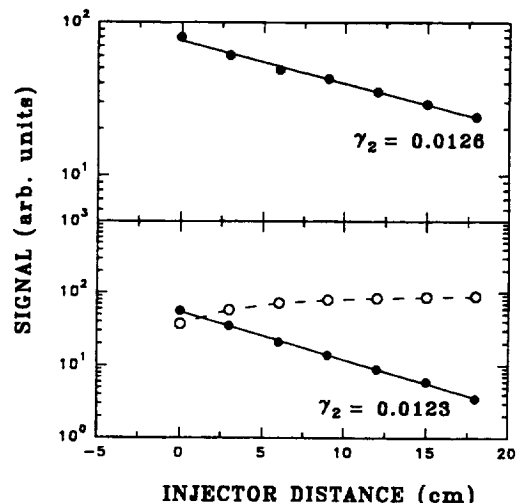


Figure 11. ClONO_2 (top) and Cl_2 (bottom, open circle) signals as a function of injector position. For the Cl_2 growth curve the first-order rate constant is calculated from the slope of a plot ($S_{\text{Cl}_2}(\infty) - S_{\text{Cl}_2}(z)$) (solid curve), where $S_{\text{Cl}_2}(\infty)$ is the Cl_2 signal at large injector distance (see text for details). Experimental conditions: $P_{\text{ClONO}_2} = 7 \times 10^{-8}$ Torr, $P_{\text{H}_2\text{O}} = 2.4 \times 10^{-4}$ Torr, $P_{\text{HCl}} = 5 \times 10^{-7}$ Torr, $P_{\text{He}} = 1.0$ Torr, velocity = 1571 cm s^{-1} , and $T = 195$ K.

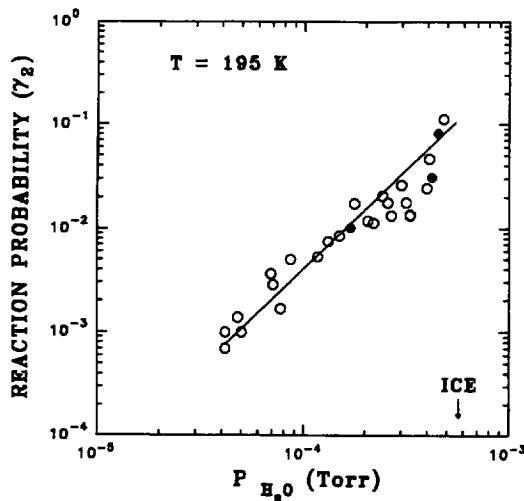


Figure 12. Reaction probability (γ_2) for reaction 2 (between ClONO_2 and HCl) as a function of $P_{\text{H}_2\text{O}}$ on SAT surfaces at 195 K. The solid curve is a fit to the experimental data in a functional form similar to eq 7 and is also summarized in Table 3. Open circles are γ_2 's determined by ClONO_2 decay, and solid circles are determined by Cl_2 growth. The ice vapor pressure at this temperature is labeled. Experimental conditions: $P_{\text{ClONO}_2} = 3 \times 10^{-8}$ – 5×10^{-8} Torr, $P_{\text{HCl}} = 4 \times 10^{-7}$ – 8×10^{-7} Torr, $P_{\text{He}} = 0.9$ – 1.0 Torr, velocity = 1300 – 1600 cm s^{-1} , and $T = 195$ K.

position at 2.6 min, both ClONO_2 and Cl_2 return within a fraction of a second to their original levels. No release of HOCl into the gas phase was observed during this process. Correcting the measured signals for relative sensitivities for detection of ClONO_2 and Cl_2 gave a Cl_2 yield of 0.9 ± 0.1 .

As is the case with the reaction between ClONO_2 and H_2O , γ_2 can be calculated both from the decay of the ClONO_2 signal and from the growth of Cl_2 as a function of the ClONO_2 injector position. In Figure 11, the first-order rate constant for Cl_2 rise (bottom, solid line) within the uncertainty of the measurement is essentially the same as that for the ClONO_2 loss (top trace).

Results for γ_2 measurements are shown in Figure 12 at 195 K as a function of the H_2O partial pressure. The temperature dependence of the γ_2 values is presented in Figure 13 for a constant H_2O partial pressure of 5.6×10^{-4} Torr. As shown in these figures, the H_2O -rich crystals show γ_2 values ≥ 0.1 , whereas the γ_2 values for the H_2SO_4 -rich crystals are more than 2 orders of

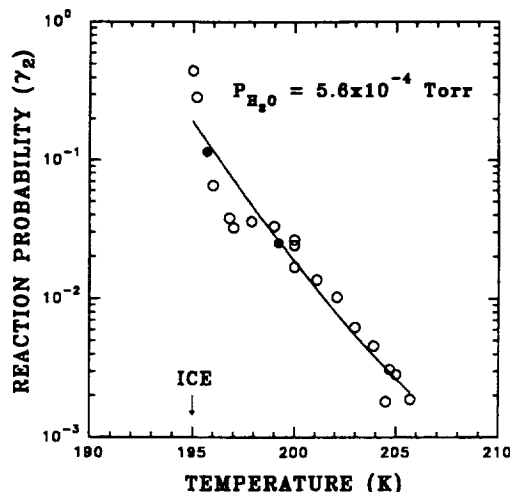


Figure 13. Reaction probability (γ_2) for reaction 2 (between ClONO_2 and HCl) as a function of temperature on SAT surfaces. Open circles are γ_2 's determined by ClONO_2 decay, and solid circles are determined by HOCl growth. The solid curve is a fit to the experimental data in a functional form similar to eq 7 and is also summarized in Table 3. The ice frost point is labeled. Experimental conditions: $P_{\text{ClONO}_2} = 3 \times 10^{-8}$ – 5×10^{-8} Torr, $P_{\text{H}_2\text{O}} = 5.6 \times 10^{-4}$ Torr, $P_{\text{HCl}} = 4 \times 10^{-7}$ – 8×10^{-7} Torr, $P_{\text{He}} = 0.9$ – 1.0 Torr, velocity = 1300 – 1600 cm s^{-1} , and $T = 195$ K.

TABLE 3: Summary and Parametrization^a of γ_2 Measurements

variable x	coefficients			experimental conditions
	a_1	a_2	a_3	
$P_{\text{H}_2\text{O}}$ (Torr)	5.25	1.91	0.00	$T = 195$ K $P_{\text{ClONO}_2} = 3 \times 10^{-8}$ – 5×10^{-8} Torr $P_{\text{HCl}} = 4 \times 10^{-7}$ – 8×10^{-7} Torr $P_{\text{He}} = 4 \times 10^{-5}$ – 5.6×10^{-4} Torr
T (K)	175.74	-1.59	0.0035	$T = 195$ – 206 K $P_{\text{ClONO}_2} = 3 \times 10^{-8}$ – 5×10^{-8} Torr $P_{\text{HCl}} = 4 \times 10^{-7}$ – 8×10^{-7} Torr $P_{\text{He}} = 5.6 \times 10^{-4}$ Torr

$$^a \log \gamma_2 = a_1 + a_2 \log x + a_3 \log^2 x.$$

magnitude smaller. Note that for the same reactant partial pressures the γ_2 on H_2O -rich SAT is ~ 0.1 at 195 K and increases slightly at 190 K (> 0.2). The parametrized temperature and $P_{\text{H}_2\text{O}}$ dependencies of γ_2 's for data shown in Figures 12 and 13 are listed in Table 3.

For all the experiments described above, initial partial pressures of HCl are always higher than those of ClONO_2 so that the pseudo-first-order assumption applies ($P_{\text{ClONO}_2} = (3$ – $5) \times 10^{-8}$ Torr and $P_{\text{HCl}} = (4$ – $8) \times 10^{-7}$ Torr). The uncertainty in the γ_2 values is approximately $\pm 30\%$ for $\gamma_2 < 0.1$; for larger γ_2 values (which are more sensitive to the gas-phase diffusion), the uncertainty is as large as a factor of 4. Some scatter in γ_2 (Figures 12 and 13) may also be due to variations in both ClONO_2 and HCl partial pressures in the various experiments.

Discussion

HCl Uptake Experiments. There have been numerous investigations of the HCl interaction with proposed PSC materials,^{21,23–25,34–39} with emphasis ranging from bulk HCl solubility to the HCl surface concentration. The nature of this process, however, is only recently beginning to be elucidated: HCl is only sparingly soluble in ice,^{37,38} but a significant amount of HCl vapor is taken up by the ice surface (corresponding to a fraction of a

monolayer coverage under stratospheric conditions).^{24,25,34,39} Similar behavior is also observed for HCl uptake on NAT.^{24,25,39} In addition, the thermodynamic state of NAT has been shown to strongly influence the HCl uptake.²⁵

As we have previously discussed,¹² the thermodynamic state of SAT is determined by two variables, e.g., either by the H₂O partial pressure at a given temperature or by the temperature at a given H₂O partial pressure. The present data show that H₂O-rich SAT surfaces take up more HCl than H₂SO₄-rich surfaces, which is expected since the chemical potential of H₂O in H₂SO₄-rich surfaces is smaller than that in H₂O-rich surfaces. Hence, the tight H₂O bonding in the H₂SO₄-rich surfaces leads to fewer free H₂O molecules available to interact with HCl molecules. The results also show that at very high HCl partial pressures ($P_{\text{HCl}} > 10^{-5}$ Torr) unlimited uptake occurs without showing HCl saturation on a time scale of several minutes, suggesting that melting occurs. These observations are qualitatively similar to the reported HCl uptake behavior on NAT.^{24,25} For the HCl uptake by ice films, our data are in reasonable agreement with that reported by Hanson and Ravishankara.²⁴

Theoretical considerations based on a physical adsorption mechanism predict an HCl uptake orders of magnitude smaller than observed on the ice surface.^{4,40} We have postulated an alternative mechanism involving the formation of a liquidlike layer on the ice surface and solvation of HCl in this layer, which is supported by thermodynamic considerations involving surface free energies.⁴ By analogy, we believe that such a mechanism most likely accounts for the observed HCl uptake on SAT reported in this study. As shown in Figure 3, the HCl uptake increases rapidly as P_{HCl} approaches the "threshold" value for melting; such a behavior would appear to indicate that the thickness of the liquidlike layer increases accordingly, as is the case with the liquidlike layer on ice as the temperature approaches 0 °C.

Leu et al.²³ and Keyser et al.⁴¹ have shown that a porosity effect related to the thickness of the substrate may significantly affect the γ values (particularly for low γ 's) as well as the HCl surface coverage, a subject which is currently in debate.^{24,42,43} We did not characterize the roughness and porosity of the SAT surfaces employed in our experiments. On the other hand, we prepared the SAT films by wetting the flow tube with 57.8 wt % H₂SO₄ solution and by subsequent freezing; visually, the films appeared smooth and uniform and were likely to be less porous than ice films formed by H₂O vapor deposition. Clearly, surface morphology studies are required to estimate the appropriate correction factors to the γ 's and to the surface coverage.

Reaction of ClONO₂ with H₂O. A wide variation of γ_1 measurements on the ice surfaces has been reported in the literature, with γ_1 's ranging from 0.009 to ≥ 0.3 .^{15–19,22,24} This discrepancy was later resolved as due to the difference in ClONO₂ partial pressures used in each of those studies:²² high ClONO₂ partial pressures in many of the early experiments led to surface saturation by HNO₃ (the reaction product) and caused deactivation of the ice surface. We also measured γ_1 's on fresh ice films at 195 K: for a ClONO₂ partial pressure range of 2×10^{-8} to 1×10^{-7} Torr, γ_1 's were found to be 0.08 ± 0.02 for an average of 15 experiments (Figure 8, open square). These values are smaller than those reported by Hanson and Ravishankara (≥ 0.3),^{22,24} considering the same level of ClONO₂ partial pressures used in both studies; they are, however, in good agreement with recent results obtained by Chu et al.⁴⁴

We also performed some experiments by first exposing fresh ice films to ClONO₂ at $\sim 10^{-7}$ Torr on a time scale of several minutes and then measuring γ_1 on such surfaces. It has been previously suggested that exposure of an ice film to ClONO₂ results in a HNO₃-doped surface, most likely in the form of NAT.^{22,24} The γ_1 's we obtained on these surfaces were on the order of 0.002 (Figure 8, solid square), similar to the results of γ_1 's measured on H₂O-rich NAT.²⁵ It is interesting to note that

for ice, H₂O-rich SAT, and H₂O-rich NAT the γ_1 values decrease in that order (Figure 8). It is likely that the presence of HNO₃ and H₂SO₄ molecules in the surface layer is responsible for this behavior: as mentioned above, HNO₃ molecules on the surface may slow reaction 1.

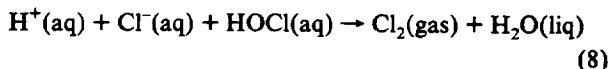
Our results show that γ_1 's depend strongly on the thermodynamic state of SAT (Figures 8 and 9): at a given temperature the γ_1 's increase with increasing H₂O partial pressure; at a given H₂O partial pressure the γ_1 's decrease with increasing temperature. This behavior is consistent with the HCl uptake discussed above, in terms of the reduced chemical potential of H₂O in H₂SO₄-rich substrate.

Lastly, there is some evidence indicating that γ_1 on H₂O-rich SAT increases slightly with decreasing temperature (see Figures 8 and 9). The same tendency was observed for the reaction between HOCl and HCl,⁴⁵ but the opposite behavior was reported for γ_1 on H₂O-rich NAT.²²

Hanson and Ravishankara⁴⁶ have very recently measured γ_1 on SAT, also as a function of $P_{\text{H}_2\text{O}}$. Their results are qualitatively in agreement with ours: the γ_1 values decrease by more than an order of magnitude for a fixed $P_{\text{H}_2\text{O}}$ as the temperature increases.

Reaction of ClONO₂ with HCl. The γ_2 's also show a strong dependence on the thermodynamic state of SAT (Figures 12 and 13), similar to that found in the HCl uptake and γ_1 experiments. For H₂O-rich SAT our measured γ_2 's are compatible with the large γ_2 values reported on H₂O-rich NAT.^{24,25} We also observed that γ_2 on H₂O-rich SAT slightly increases with decreasing temperature for the same reactant partial pressures ($\gamma_2 = 0.12$ at 195 K and $\gamma_2 \geq 0.3$ at 190 K).

It was previously suggested that on water ice and H₂O-rich NAT reaction 2 involves a two-step process which consists of reaction 1 followed by reaction 3.^{24,45} We believe that such a process also applies for reaction 2 on SAT: both reduced HCl surface concentrations and small γ_1 's for H₂SO₄-rich SAT lead to the reduced γ_2 's; reaction 3 also enhances reaction 1 by refreshing the SAT surface with H₂O. We have recently proposed that a more realistic mechanism for reaction 3 includes the following ionic reaction, which occurs after HCl uptake and solvation in the liquidlike layer:^{13,47}



Eigen and Kustin investigated this reaction at 298 K;⁴⁸ its rate is likely to be close to the diffusion limit in the liquidlike layer, which is highly acidic.

As is the case with γ_1 , Hanson and Ravishankara's recent measurements⁴⁶ of γ_2 are also qualitatively in agreement with our measured values, the γ_2 changing strongly with temperature at a fixed $P_{\text{H}_2\text{O}}$. (The two sets of results were obtained using different P_{HCl} and $P_{\text{H}_2\text{O}}$.)

Stratospheric Implications

Earlier studies^{12–14} have shown that SAT may form and persist at temperature and H₂O partial pressure conditions typical of the high-latitude stratosphere: once crystallized, those aerosols are stable until they melt at ~ 215 K or are removed from the stratosphere by scavenging or by acting as condensation nuclei in the formation of PSCs. Those studies¹³ also suggest that in the stratosphere, considering a constant ambient H₂O mixing ratio, the thermodynamic state of frozen sulfate aerosols is determined only by temperature. For most of experiments reported here, the gas-phase HCl and ClONO₂ concentrations are maintained at levels that are representative of the stratosphere, and hence the measurements are directly applicable to the stratosphere.

Our results show that at an ambient stratospheric H₂O partial pressure of 3.4×10^{-4} Torr (~ 5 ppmv H₂O mixing ratio at 100 mb) HCl uptake by frozen sulfate aerosols approaches a tenth

of a monolayer coverage ($\sim 10^{14}$ molecules cm^{-2}) at low temperatures ($T < 195$ K) whereas only a very small amount of HCl ($< 10^{12}$ molecules cm^{-2}) is taken up at temperatures higher than 200 K. For reaction 1, γ_1 is observed to be on the order of 0.02 at low temperature ($T < 195$ K) and less than 0.002 at temperatures above 205 K. Similarly, γ_2 is found to be greater than 0.2 at low temperatures ($T < 195$ K) and decreases substantially with increasing temperature. These results imply that in the stratosphere the heterogeneous interactions between ClONO₂ and HCl on frozen sulfate aerosols are largely governed by the temperature: they proceed efficiently at low temperatures ($T < 195$ K) and less efficiently when the temperature is higher ($T > 205$ K). Hence, chlorine activation should occur readily on frozen sulfate aerosols in the winter polar stratosphere, even in the absence of PSCs.

Summary

In this paper we have presented measurements of the heterogeneous interactions of ClONO₂ and HCl on sulfuric acid tetrahydrate surfaces. The results indicate that the reaction probabilities for (1) and (2) as well as the HCl uptake depend strongly on the thermodynamic state of the SAT substrate, with the H₂O-rich forms being more reactive than H₂SO₄-rich forms. In the stratosphere these reactions should proceed efficiently at low temperatures ($T < 200$ K) and, hence, play an important role in chlorine activation at high latitudes in the winter.

Acknowledgment. This research was supported by an NSF grant (ATM-9017150) and a NASA grant (NAG2-632) to the Massachusetts Institute of Technology. Helpful discussions on this subject with M. T. Leu are greatly appreciated. R.Z. is supported by a NASA graduate fellowship.

References and Notes

- (1) Solomon, S. *Rev. Geophys.* 1988, 26, 131.
- (2) Anderson, J. G.; Toohey, D. W.; Brune, W. H. *Science* 1991, 251, 39.
- (3) Brune, W. H.; Anderson, J. G.; Toohey, W. D.; Fahey, D. W.; Kawa, S. R.; Jones, R. L.; McKenna, D. S.; Poole, L. R. *Science* 1991, 252, 1260.
- (4) Molina, M. J. In *CHEMRAWN VII: Chemistry of the Atmosphere: The Impact of Global Change*; Calvert, J. G., Ed.; Blackwell Sci. Publ.: Oxford, in press.
- (5) Toon, O. B.; Hamill, P.; Turco, R. P.; Pinto, J. *Geophys. Res. Lett.* 1986, 13, 1283.
- (6) Crutzen, P. J.; Arnold, F. *Nature* 1986, 324, 651.
- (7) Poole, L. R.; McCormick, M. P. *J. Geophys. Res.* 1987, 93, 8423.
- (8) Hamill, P.; Turco, R. P.; Toon, O. B. *J. Atmos. Chem.* 1988, 7, 287.
- (9) Steele, H. M.; Hamill, P.; McCormick, M. P.; Swissler, T. J. *J. Atmos. Sci.* 1983, 40, 2055.
- (10) Zhang, R.; Wooldridge, P. J.; Molina, M. J. *J. Phys. Chem.* 1993, 97, 8541.
- (11) Toon, O.; Browell, E.; Gary, B.; Bait, L.; Newman, P.; Pueschel, R.; Russel, P.; Schober, M.; Toon, G.; Traub, W.; Valero, F.; Selkirk, H.; Jordan, J. *Science* 1993, 261, 1136.
- (12) Zhang, R.; Wooldridge, P. J.; Abbott, J. P. D.; Molina, M. J. *J. Phys. Chem.* 1993, 97, 7351.
- (13) Molina, M. J.; Zhang, R.; Wooldridge, P. J.; McMahon, J. R.; Kim, J. E.; Chang, H. Y.; Beyer, K. D. *Science* 1993, 261, 1481.
- (14) Middlebrook, A. M.; Iraci, L. T.; McNeill, L. S.; Koehler, B. G.; Saastad, O. W.; Tolbert, M. A. Submitted to *J. Geophys. Res.*
- (15) Molina, M. J.; Tso, T.; Molina, L. T.; Wang, F. C. Y. *Science* 1987, 238, 1253.
- (16) Tolbert, M. A.; Rossi, M. J.; Malhotra, R.; Golden, D. M. *Science* 1987, 238, 1258.
- (17) Tolbert, M. A.; Rossi, M. J.; Golden, D. M. *Science* 1988, 240, 1018.
- (18) Leu, M. T. *Geophys. Res. Lett.* 1988, 15, 17.
- (19) Leu, M. T. *Geophys. Res. Lett.* 1988, 15, 851.
- (20) Quinlan, M. A.; Reihl, C. M.; Golden, D. M.; Tolbert, M. A. *J. Phys. Chem.* 1990, 94, 3255.
- (21) Moore, S. B.; Keyser, L. F.; Leu, M.-T.; Turco, R. P.; Smith, R. H. *Nature* 1990, 345, 333.
- (22) Hanson, D. R.; Ravishankara, A. R. *J. Geophys. Res.* 1991, 96, 5081.
- (23) Leu, M. T.; Moore, S. B.; Keyser, L. F. *J. Phys. Chem.* 1991, 95, 7763.
- (24) Hanson, D. R.; Ravishankara, A. R. *J. Phys. Chem.* 1992, 96, 2682.
- (25) Abbott, J. P. D.; Molina, M. J. *J. Phys. Chem.* 1992, 96, 7674.
- (26) Hanson, D. R.; Ravishankara, A. R. *J. Geophys. Res.* 1991, 96, 17, 307.
- (27) Golden, D. M.; Manion, J. A.; Reihl, C. M.; Tolbert, M. A. In *CHEMRAWN VII: Chemistry of the Atmosphere: The Impact of Global Change*; Calvert, J. G., Ed.; Blackwell Sci. Publ.: Oxford, in press.
- (28) Gable, C. M.; Betz, H. F.; Maron, S. H. *J. Am. Chem. Soc.* 1950, 72, 1445.
- (29) Brown, R. L. *J. Res. Natl. Bur. Stand. (U.S.)* 1978, 83, 1.
- (30) Hirshfelder, J. O.; Curtiss, C. F.; Bird, R. B. *Molecular Theory of Gases and Liquids*; Wiley and Sons: New York, 1954.
- (31) Schack, C. *J. Inorg. Chem.* 1967, 6, 1938.
- (32) DeMore, W. B.; Sander, S. P.; Golden, D. M.; Molina, M. J.; Hampson, R. F.; Kurylo, M. J.; Howard, C. J.; Ravishankara, A. R. Chemical kinetics and photochemical data for use in stratospheric modeling; JPL Publ. 90-1, NASA, 1990.
- (33) Jansco, G.; Pupezin, J.; Van Hook, W. A. *J. Phys. Chem.* 1970, 74, 2984.
- (34) Abbott, J. P. D.; Beyer, K. D.; Fucaloro, A. F.; McMahon, J. R.; Wooldridge, P. J.; Zhang, R.; Molina, M. J. *J. Geophys. Res.* 1992, 97, 15, 819.
- (35) Hanson, D.; Mauersberger, K. *Geophys. Res. Lett.* 1988, 15, 1507.
- (36) Wofsy, S. C.; Molina, M. J.; Salawitch, R. L.; Fox, L. E.; McElroy, M. B. *J. Geophys. Res.* 1988, 93, 2442.
- (37) Elliott, S.; Turco, R. P.; Toon, O. B.; Hamill, P. *Geophys. Res. Lett.* 1990, 17, 425.
- (38) Marti, J.; Mauersberger, K.; Hanson, D. *Geophys. Res. Lett.* 1991, 18, 1861.
- (39) Chu, L. T.; Leu, M. T.; Keyser, L. F. *J. Phys. Chem.* 1993, 97, 7779.
- (40) Kroes, G. J.; Clary, D. C. *Geophys. Res. Lett.* 1992, 19, 1355.
- (41) Keyser, L. F.; Moore, S. B.; Leu, M.-T. *J. Phys. Chem.* 1991, 95, 5496.
- (42) Keyser, L. K.; Leu, M. T.; Moore, M. B. *J. Phys. Chem.* 1993, 97, 2800.
- (43) Hanson, D. R.; Ravishankara, A. R. *J. Phys. Chem.* 1993, 97, 2802.
- (44) Chu, L. T.; Leu, M. T.; Keyser, L. F. Submitted to *J. Phys. Chem.*
- (45) Abbott, J. P. D.; Molina, M. J. *Geophys. Res. Lett.* 1992, 19, 461.
- (46) Hanson, D. R.; Ravishankara, A. R. *J. Geophys. Res.*, in press.
- (47) Molina, M. J. In *The Tropospheric Chemistry of Ozone in the Polar Regions*; Niki, H., Becker, K. H., Eds.; Springer-Verlag: New York, 1993.
- (48) Eigen, M.; Kustin, K. *J. Am. Chem. Soc.* 1961, 84, 1355.